

Article

Buckling Analysis of Conical Shell Openings with Reinforced Perimeter Walls under Uniform External Pressure

Lin Yue , Hongzhang Pan, Yongmei Zhu *, Tianyi Sun and Jian Zhang 

School of Mechanical Engineering, Jiangsu University of Science and Technology, Zhenjiang 212003, China

* Correspondence: zymtt@163.com

Abstract: In this paper, the effects of opening parameters and reinforcing wall parameters on the bearing capacity of conical shells with an opening were investigated. Under the condition that the conical shells with an opening were all reinforced with walls, the opening position and the inclination angle of the reinforced wall were selected as variables to be used in the numerical analysis and hydrostatic pressure test. The nonlinear numerical buckling load and the test results were compared. The difference was within 17.8%, which verified the rationality of the finite element model. The final buckling mode obtained by numerical calculation of the measured data was in good agreement with the real collapse mode obtained by hydraulic testing of the actual model. Then the influence of the opening position and inclination angle of the reinforcing wall on the buckling load of the conical shell under different opening rates was analyzed in detail.

Keywords: conical shell; opening; opening position; reinforcing wall inclination angle; external pressure



Citation: Yue, L.; Pan, H.; Zhu, Y.; Sun, T.; Zhang, J. Buckling Analysis of Conical Shell Openings with Reinforced Perimeter Walls under Uniform External Pressure. *Metals* **2023**, *13*, 824. <https://doi.org/10.3390/met13050824>

Academic Editor: Alireza Akhavan-Safar

Received: 2 March 2023

Revised: 17 April 2023

Accepted: 18 April 2023

Published: 23 April 2023



Copyright: © 2023 by the authors. Licensee MDPI, Basel, Switzerland. This article is an open access article distributed under the terms and conditions of the Creative Commons Attribution (CC BY) license (<https://creativecommons.org/licenses/by/4.0/>).

1. Introduction

As a common pressure vessel, the pressure cabin is the core structural component to ensure the safety of internal equipment. The design and manufacture of the pressure shell structure are very important. Its strength and stability are the issues that need to be focused on [1]. A rotary shell structure with high load-bearing efficiency has the advantage of good streamline. It is widely used in aviation, marine, and other engineering fields [2]. The conical pressure shell, as one of the typical reverting pressure shells, is widely used in the tail section of marine submersibles and submarines, the main part of deep-sea workstations, aerospace return capsules, pressure vessels, and other structures [3–6].

Many parameters affect the buckling performance of conical shells. B.S. Golzan et al. [7] studied the nonlinear response of truncated conical shells; shallow conical caps subjected to external uniform pressure are discussed when discharging liquids or wind loads. It is concluded that the buckling ability of shells depends on two main geometric ratios: the length-radius ratio (L/R) and the thickness-radius ratio (t/R). Sang-Rai Cho et al. [8] studied experimental and numerical investigations on the ultimate strength of steel-welded, ring-stiffened conical shells under external hydrostatic pressure. By varying the basic geometry, such as the conical angle and stiffener size and spacing, the numerical results were in good agreement with the experimental results. In the actual situation, due to the needs of the engineering structure, it is necessary to design the opening structure on the pressure shell, such as the entrance door, the safety door, the observation window, and so on. Openings will lead to reduced strength, stability, and stress concentration. Therefore, it is inevitable to select the opening parameters of the pressure shell with openings and evaluate the strength. Wu et al. [9] studied the interaction of opening diameter, reinforcing rib size, and the number of ribs on a conical shell under the opening. That is, when the radius of the opening increased, the closer the opening edge was to the rib, the more obvious the reinforcing effect of the rib on the opening was. M. Kathiresan [10] experimentally and numerically studied the effects of different shapes, sizes, and numbers of lateral cutouts at

various locations on the load-bearing capacity, buckling behavior, and energy absorption characteristics of aluminum cones under a quasi-static axial load. The results showed that, regardless of the shape, size, and number of notches, changing the notch's position from the middle height to three-quarters of the bottom resulted in a reduction in bearing capacity. The energy absorption characteristics of a conical truncated cone with a circular incision are better than those of a conical truncated cone with square or trapezoidal incisions at the same position. Hubert Debski [11] et al. studied the impact of eccentric loads on the buckling characteristics of composite materials, causing structural load-bearing capacity loss, and investigated the effects of laminated and cross-sectional shapes on the buckling load, post-buckling equilibrium path, and failure load of compressed structures. Research has shown that composite structures can operate in a post-buckling state, and the eccentric compression load parallel to the test profile has a negative impact on their stability and load-bearing capacity. The increase in buckling load will reduce the compression of the profile web. P. Rozylo [12] analyzed the failure phenomenon of axially compressed thin-walled composite structures with channel shapes and analyzed the failure phenomenon of axially compressed thin-walled composite structures with channel shapes. At present, the research on the complete conical shell shows that the buckling performance of the cone shell mainly depends on factors such as the length-diameter ratio, diameter-thickness ratio, and cone angle. Regarding the conical shell of the open hole, there is a study of the shape of the open hole, and there is a study of rib strengthening for the open hole conical shell. All of them are relatively innovative research ideas that provide certain reference opinions for other articles.

At present, most of the studies focus on small openings and strengthening the wall orthogonal to the openings, and the main research object is the buckling characteristics analysis of complete conical shells and ribbed conical shells, ignoring the influence of the inclined wall on the bearing capacity of the conical shell. At the same time, the influence of large openings and opening positions is also rare. The main focus of this article is on the analysis of the mechanical characteristics of reinforced conical shells with openings, and the impact of the angle of inclination of the reinforced wall on the nonlinear buckling of conical shells is mainly analyzed, which is the main novelty in relation to the current works in the literature on the subject. In this paper, ten stainless steel open-reinforcement conical shells with different opening positions and inclined angles of the wall were fabricated. The thickness test and three-dimensional scanning of the geometric shape were carried out. The buckling performance analysis was carried out using finite element numerical analysis and a hydrostatic pressure experiment. Then, the finite element calculation was carried out in detail based on different inclined angles and opening positions of the reinforcing wall, and its influence on the mechanical properties of the conical shell was analyzed.

2. Materials and Methods

2.1. Conical Shell Opening Reinforcement

In this paper, there are a total of ten stainless steel wall reinforcement conical shells with an opening for the experimental study. The inclination angles of the reinforced wall were selected as 0° , 15° and 30° , and the opening positions are $1/4$, $2/4$, and $3/4$ of the conical shell generatrix, respectively. Each group has two sample models. The basic dimensions of the conical shell are: the diameters of the small end and the large end of the conical shell is $D_1 = 76$ mm, $D_2 = 128$ mm, the wall thickness of the conical shell is $t = 1$ mm, the length of the conical shell is $L = 150$ mm, and the opening diameter of the conical shell is $d_0 = 30$ mm. The reinforced enclosure in this paper is a cylindrical shell enclosure; the thickness of the enclosure is different from the thickness of the conical shell; the whole is cylindrical, penetrated by the opening, and divided into two parts: inner and outer. The parameters of the reinforced wall of the conical shell are the wall thickness $t_0 = 1.2$ mm, and the wall height $H = 40$ mm, respectively. H_1 is the height inside the enclosure; H_2 is the height outside the enclosure; $H_1 = H_2 = 20$ mm. Table 1 shows the geometric parameters of conical shells with an opening, and Figure 1 shows the schematic diagram of the two

conical shells, where α is the angle between the center line of the reinforced wall and the normal line of the conical shell.

Table 1. The geometric parameters of conical shells with an opening.

Sample	d_0 (mm)	H_1 (mm)	H_2 (mm)	α (mm)	Opening Position
CS-1/4-0	30	20	20	0	1/4
CS-2/4-0	30	20	20	0	2/4
CS-3/4-0	30	20	20	0	3/4
CS-2/4-15	30	20	20	15	2/4
CS-2/4-30	30	20	20	30	2/4

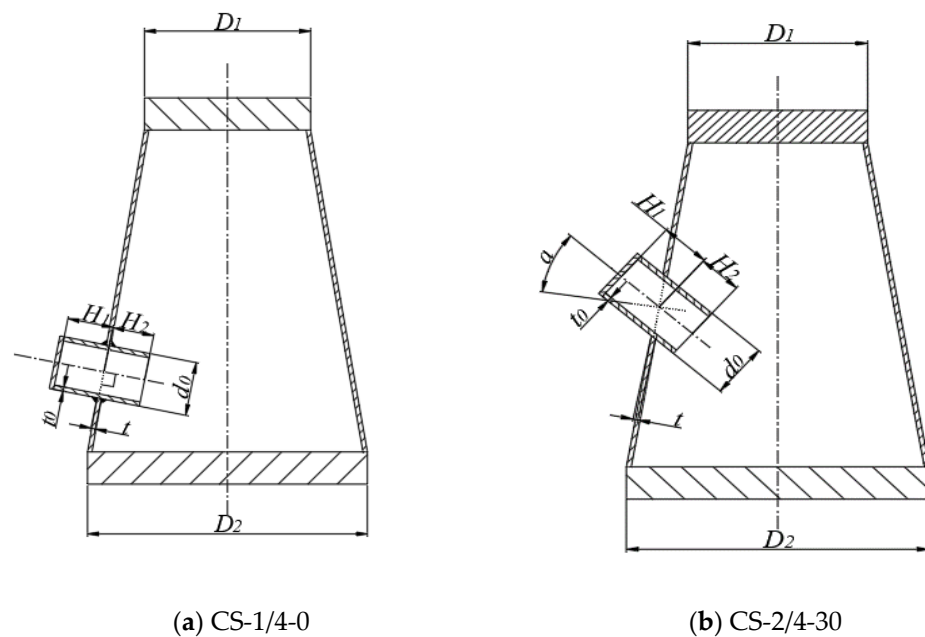


Figure 1. The structure of the conical shell with an opening: (a) the conical shell with 1/4 position and an angle of 0° ; (b) the conical shell with 2/4 position and an angle of 30° .

2.2. Geometry and Manufacturing Process

The test models were fabricated according to the above dimensions. Firstly, the 304 stainless steel plate with a nominal thickness of 1 mm was cut and rolled. The two ends of the rolled sample were welded by tungsten inert gas butt welding, and then the hole was opened at the set position. Then, use a 304 stainless steel plate with a nominal thickness of 1.2 mm to roll the welded cylinder as a reinforcing wall. Finally, the large and small ends of the conical shell model and one end of the cylindrical wall were welded to seal. The thickness of the head ($t_1 = 15$ mm) was set to 15 times the thickness of the conical shell. The conical shell models were polished after welding. Ten test models are shown in Figure 2.



Figure 2. The test models. (a) CS-1/4-0-1, (b) CS-1/4-0-2, (c) CS-2/4-0-1, (d) CS-2/4-0-2, (e) CS-3/4-0-1, (f) CS-3/4-0-2, (g) CS-2/4-15-1, (h) CS-2/4-15-2, (i) CS-2/4-30-1, (j) CS-2/4-30-2.

3. Prediction and Test Data

3.1. Measurement and Geometric Analysis

Firstly, the geometric measurement of the conical shell was carried out, and the measured thickness data provided the parameters for the subsequent finite element simulation. Each conical shell with an opening had 80 measuring points. Eight points were distributed 45° apart along the circumference, and ten points were distributed uniformly along the axis, totaling 80 measurement points, as shown in Figure 3. As shown in Figure 4, the equipment used was an ultrasonic thickness gauge. The working principle was to use the pulse reflection of an ultrasonic wave in the medium to test the thickness of the object, and the measurement accuracy was ± 0.001 mm. The thickness gauge probe was coated with an ultrasonic coupling agent before measurement. When the thickness gauge signal reaches full scale or only one full-scale difference, the reading and recording are performed. The measurement results are shown in Table 2, where t_0 was the nominal wall thickness, t_{max} was the maximum wall thickness, t_{min} was the minimum wall thickness, t_{ave} was the average wall thickness, and t_{std} was the thickness standard deviation. Figure 5 shows the measurement thickness diagram of CS-/2-0-1.

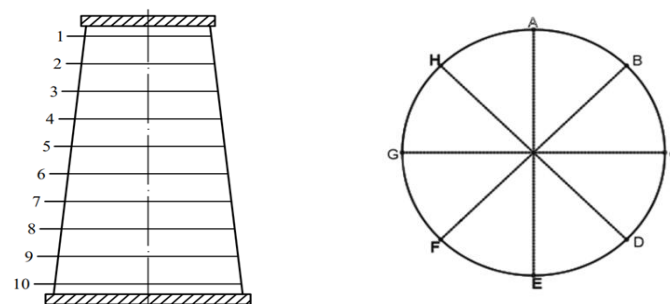


Figure 3. Distribution of the wall thickness measurement points of the test.



Figure 4. Sample model actual thickness measurement.

Table 2. Measurement results of the ten test models.

Sample	t_{min}	t_{av}	t_{max}	t_{std}
	(mm)			
CS-1/4-0-1	0.684	0.804	0.924	0.052
CS-1/4-0-2	0.697	0.825	0.952	0.046
CS-2/4-0-1	0.657	0.779	0.901	0.032
CS-2/4-0-2	0.782	0.853	0.923	0.029
CS-3/4-0-1	0.620	0.690	0.760	0.038
CS-3/4-0-2	0.647	0.729	0.810	0.035
CS-2/4-15-1	0.635	0.920	0.779	0.040
CS-2/4-15-2	0.684	0.763	0.841	0.047
CS-2/4-30-1	0.697	0.745	0.793	0.041
CS-2/4-30-2	0.612	0.698	0.783	0.037

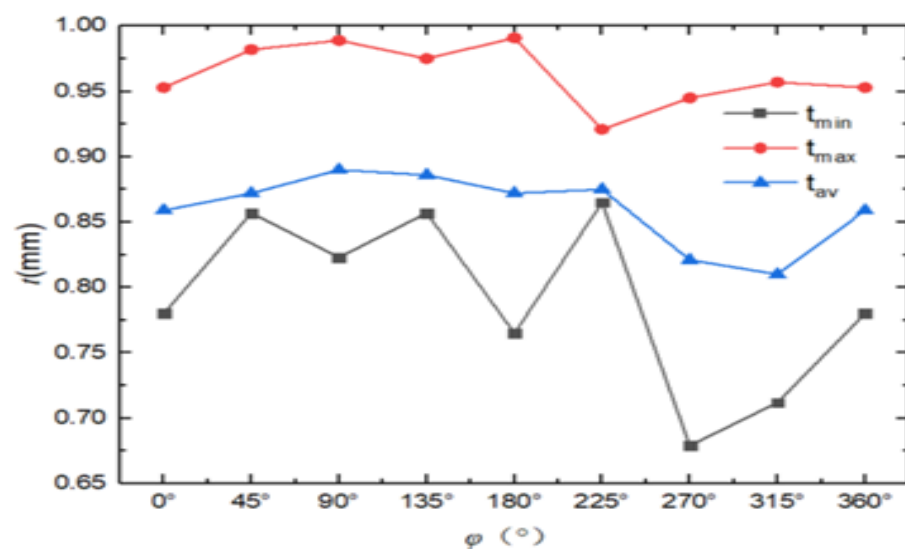


Figure 5. Thickness distribution diagram of CS-/2-0-1.

The minimum, maximum, average, and standard deviation data of the wall thickness of the ten conical shell samples are listed in Table 2. The errors of the minimum thickness and the maximum thickness of the ten conical shell models are in the range of 0.148 to 0.340 mm. The average thickness varies in the range from 0.690 to 0.920 mm, and the thickness standard deviation varies in the range from 0.029 to 0.052 mm. These errors may have been caused by the model during the production process. These errors do not affect the rationality of the analysis results, and the analysis results still have reference values.

After measuring the thickness, because there may be pits caused by damage or collision during the processing, these may affect the results of subsequent tests, so it is necessary to perform three-dimensional scanning on the processed conical shell model before the hydraulic test. Before scanning, the model was simply cleaned, and the scanning mark points were attached to the model. The equipment used in this three-dimensional scanning was the handheld three-dimensional scanner of Shining 3D Pro 3D Company, and the scanning accuracy was 0.02 mm. After scanning the model, the redundantly scanned unwanted areas were removed through the splicing of marker points, feature splicing, mixed splicing, and cutting, and finally, the required point cloud data of the entire model surface was obtained. Then, the real geometric contour of the actual model was obtained by the reverse engineering modeling software Geomagic Studio. The scanned model was seamed, the redundant discrete points were removed, and the local coordinate system was attributed to the normal position. Finally, a complete three-dimensional point cloud model was obtained. The scanning process was shown in Figure 6.



Figure 6. Three-dimensional scanning.

After scanning, the head used for sealing does not participate in the actual finite element simulation calculation. Therefore, it is necessary to cut the head with Geomagic Studio software. After cutting the head, it is imported into Gom Inspect for contour surface deviation analysis with the ideal model, and the comparative analysis results are shown in Figure 7. Figure 7 is the contour contrast error cloud diagram of the model. The legend in the figure represents the shape error and error frequency of the real and ideal cylindrical shell models.

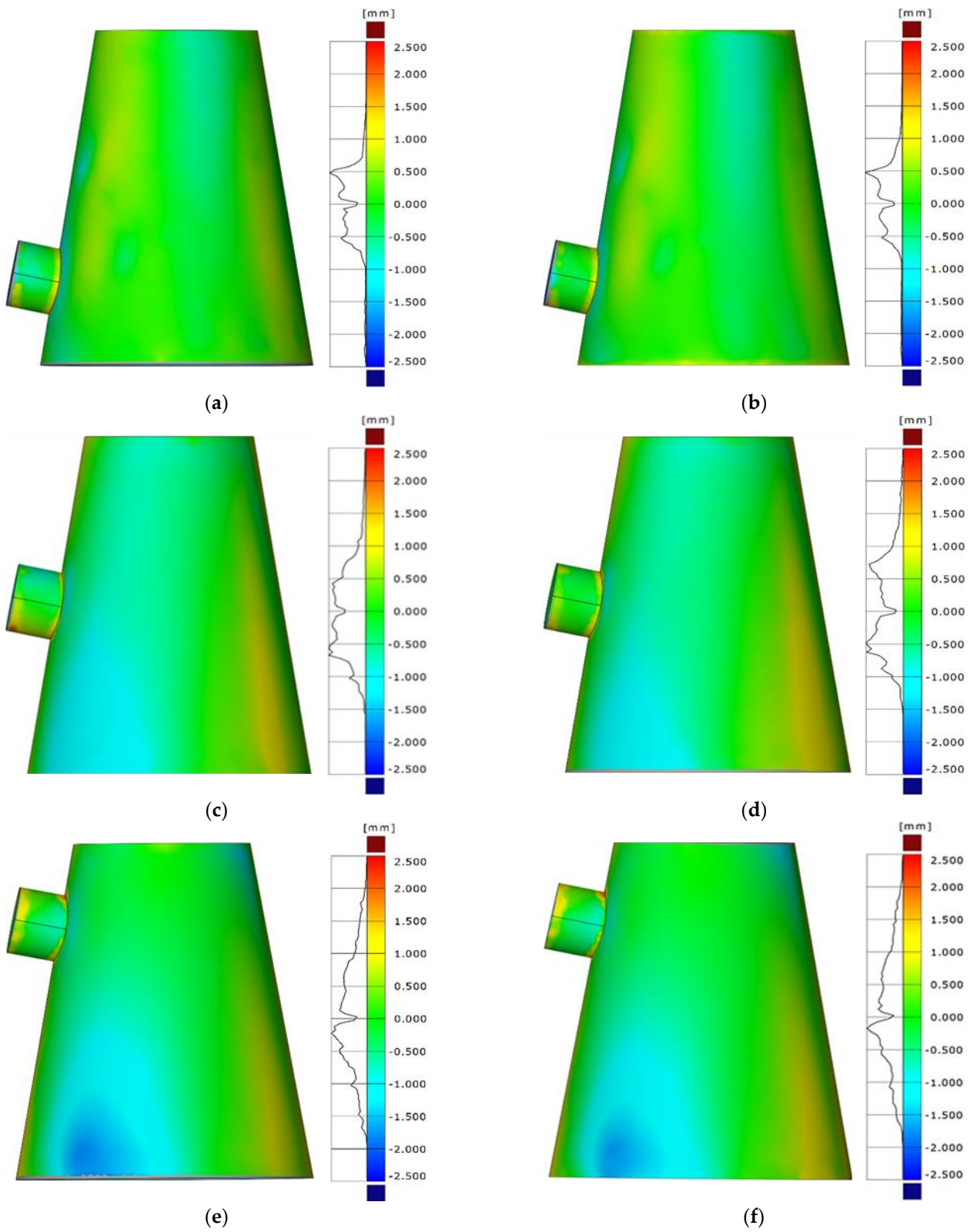


Figure 7. Cont.

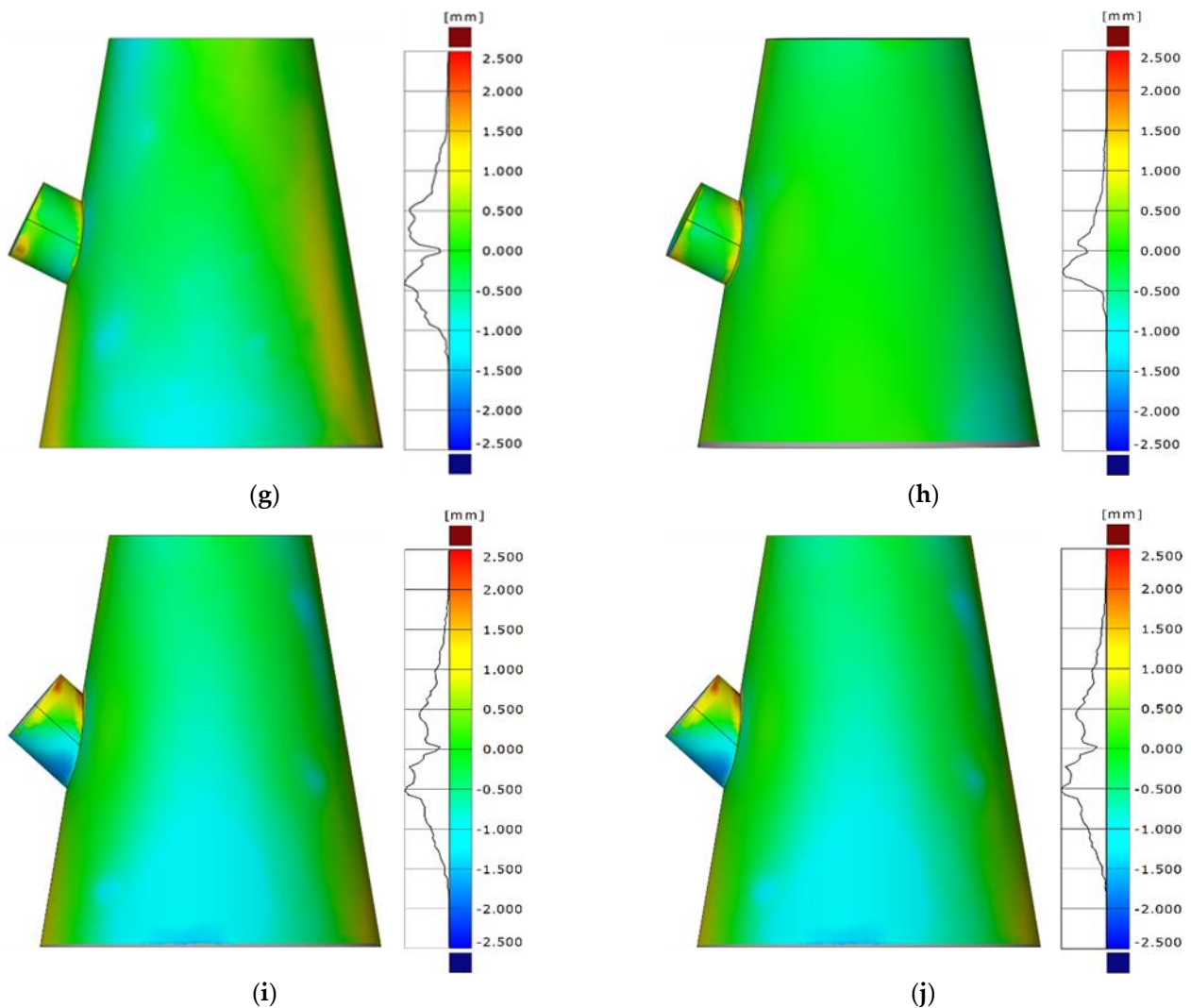


Figure 7. Fabrication deviations of the test models from perfect geometries. (a) CS-1/4-0-1, (b) CS-1/4-0-2, (c) CS-2/4-0-1, (d) CS-2/4-0-2, (e) CS-3/4-0-1, (f) CS-3/4-0-2, (g) CS-2/4-15-1, (h) CS-2/4-15-2, (i) CS-2/4-30-1, (j) CS-2/4-30-2.

From Figure 7, it can be seen that the deviation between the 10 test models and the theoretical model is small in general. The main errors in the ten test models are in the opening reinforcement and the conical shell bus weld, and the remaining surfaces are in good agreement with the theoretical model. Due to the limitations of processing conditions and uncontrollable factors, there is little difference between the experimental model and the theoretical model, but it can still provide a reference for the stability test of conical shell opening reinforcement.

3.2. Experiment

After the measurement and scanning, the hydraulic test was carried out on each specimen. After the test, the water pressure curve of each model was obtained. Considering the buckling load obtained by simulation is small, a pressure chamber with a range of 8 MPa was selected. The preparation steps and procedures for the hydrostatic test were described in detail in previous reports [13–15]. The damaged conical shell was shown in Figure 8, in which the CS-3/4-0-2 model fails to leak water and the other models are normal without leakage. Table 3 was the hydrostatic test data table for ten conical shells, and the recorded pressure curve was shown in Figure 9.



Figure 8. Conical shells with an opening after failure. (a) CS-1/4-0-1, (b) CS-1/4-0-2, (c) CS-2/4-0-1, (d) CS-2/4-0-2, (e) CS-3/4-0-1, (f) CS-3/4-0-2, (g) CS-2/4-15-1, (h) CS-2/4-15-2, (i) CS-2/4-30-1, (j) CS-2/4-30-2.

Table 3. Test results of ten conical shells.

Sample	P_{1-test} (MPa)	P_{2-test} (MPa)	$P_{test-ave}$ (MPa)
CS-1/4-0	1.624	1.764	1.694
CS-2/4-0	1.792	1.953	1.873
CS-3/4-0	1.542	-	1.542
CS-2/4-15	2.034	2.213	2.124
CS-2/4-30	2.326	2.435	2.381

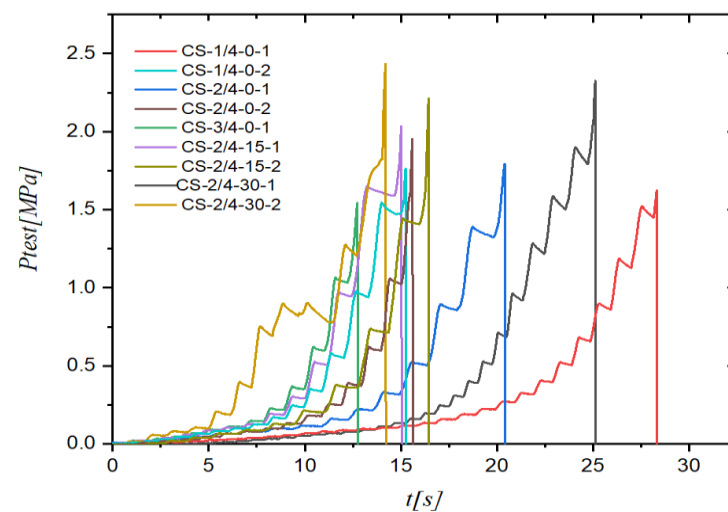


Figure 9. Hydrostatic pressure curves for the shell samples.

From Figure 8, it can be seen that the test models of 10 conical shells all show the failure form of local depression, and the failure positions are similar, being basically distributed near the equator and mostly on the opposite side of the reinforced wall of the conical shell,

that is, near the weld (red solid line). It is consistent with the failure mode of a conical shell and a cylindrical shell under external pressure [16,17].

It can be seen from Table 3 that when the reinforced wall is perpendicular to the generatrix ($\alpha = 0^\circ$), the bearing capacity of the opening position at the 2/4 position is between 10.6% and 21.5% higher than that of the opening position at the 1/4 position and 3/4 position. The bearing capacity of the opening position at 1/4 of the generatrix (near the small end) is 9.9% higher than that of the opening position at 3/4 of the generatrix (near the large end). When the opening position is 2/4 and $\alpha = 30^\circ$, the ultimate load of the conical shell is the largest, which is 12.1% and 27.1% higher than that of $\alpha = 15^\circ$ and $\alpha = 0^\circ$.

Figure 9 records the changing trend of the pressure curve of the conical shell during the test under hydrostatic pressure. It can be seen from the curve that the pressurization time is basically within 30 s and that the pressurization trend is slowly rising first and then rapidly increasing until the maximum critical buckling load.

4. Results and Discussion

4.1. Comparison of Experimental and Numerical Analysis

The conical shell model was first built on ABAQUS. The point cloud model scanned in Section 3.1 is imported into ABAQUS to be uniformly thickened. The thickness is the average thickness of the actual measurement of each model. Each model has the same material properties: Young's modulus $E = 200$ GPa, Poisson's ratio $\mu = 0.291$, yield strength $\sigma_y = 628$ MPa, mass density $\rho = 7930$ kg/m³. Then the model is divided into grids, which are all composed of S4 and S3 grid types. The grid size is determined by the grid density convergence analysis method, and the mesh length cannot exceed $0.5\sqrt{Rt}$ [18]. The same boundary condition setting and loading method are used for each conical shell structure model [19]. One end of the conical shell is fully constrained, and the other end retains axial movement. The outer surface is subjected to $P_0 = 1$ MPa uniform external pressure load. The boundary conditions and loading are shown in Figure 10.

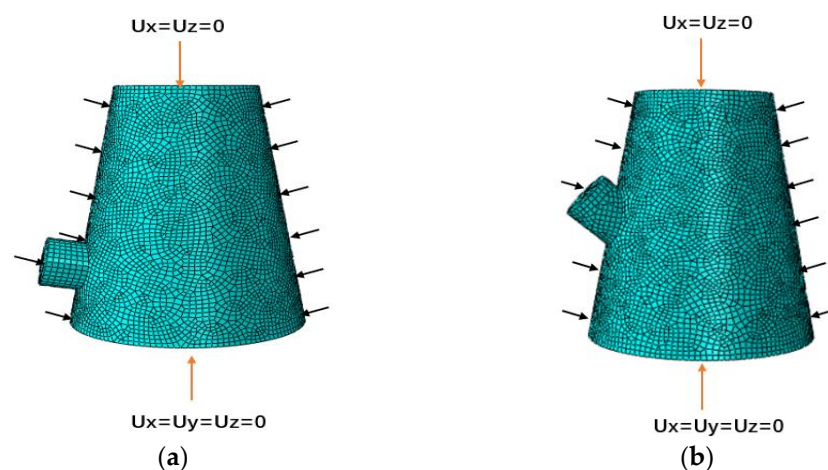


Figure 10. Mesh and boundary constraint modes of the numerical model: (a) the conical shell with 1/4 position and an angle of 0° ; and (b) the conical shell with 2/4 position and an angle of 30° .

The nonlinear finite element analysis of the conical shell model is carried out. The risk analysis method is used here. The Riks method is mainly used to solve the material and geometric nonlinear buckling, and the critical buckling load of the conical shell is determined by the LPF curve. In this nonlinear calculation, the real scanning model is used to carry out the finite element method of calculation on the actual model with real defects. In this experiment, the initial arc length is 0.1 mm, the minimum arc length is 0.00001 mm, the maximum arc length is 0.5 mm, and the total arc length iteration step is 100 steps. Figure 11 shows the equilibrium path, critical buckling mode, and post-buckling mode for CS-2/4-30-1. Table 4 shows the numerical results and test results of 10 test models.

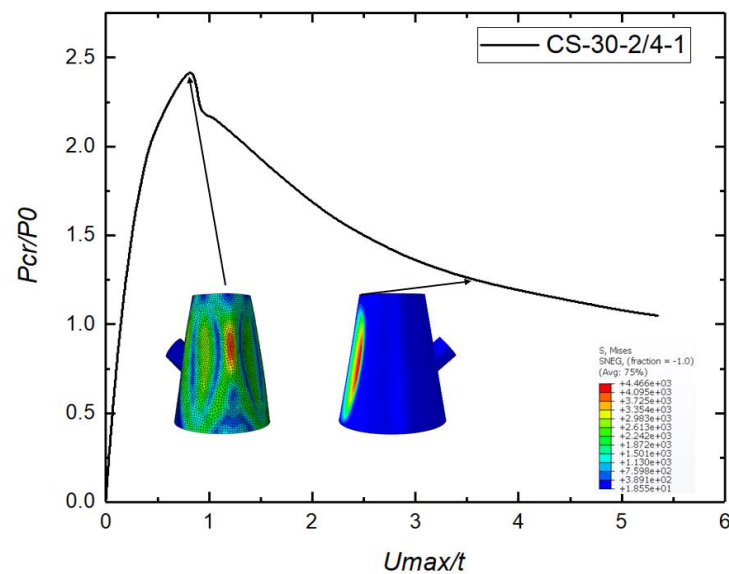


Figure 11. Equilibrium path, critical buckling mode, and post-buckling mode for CS-2/4-30-1: P_{cr}/P_0 is the ratio of the applied external load to the initial load ($P_0 = 1$ MPa), and U_{max}/t is the ratio of the maximum deformation U_{max} to the nominal shell thickness t .

Table 4. Numerical analysis results.

Name	P_{ABAQUS} (MPa)	P_{test} (MPa)	P_{ABAQUS}/P_{test}
CS-2/4-0-1	1.845	1.702	1.084
CS-2/4-0-2	1.857	1.953	0.951
CS-1/4-0-1	1.715	1.624	1.056
CS-1/4-0-2	1.732	1.764	0.982
CS-3/4-0-1	1.780	1.542	1.154
CS-2/4-15-1	2.396	2.034	1.178
CS-2/4-15-2	2.413	2.213	1.090
CS-2/4-30-1	2.412	2.326	1.037
CS-2/4-30-2	2.384	2.435	0.979

It can be seen from Figure 11 that as the deflection increases, the applied pressure increases monotonically at first, but after reaching its peak, the pressure decreases greatly. The failure mode of the opening reinforced conical shell is local depression, which is basically consistent with the collapse mode of the corresponding test model, indicating that the hydrostatic test results are in good agreement with the numerical analysis results.

According to Table 4, it can be seen that among the 10 conical shells, except that the failed CS-0-3/4-2 is not included, the maximum difference between the numerical results and the test results is 17.8%, and the minimum difference is 1.80%. This difference may be attributed to the 304 stainless steel material's properties of having small differences. The results show that the nonlinear critical buckling load of the conical shell with an opening can be obtained based on the actual geometric shape, the average thickness, and material properties.

4.2. The Effect of Opening Position on Critical Buckling Load under Different Apertures

This section mainly discusses the effect of opening position and opening size on the stability of conical shells. The reinforced wall is set perpendicular to the generatrix of the conical shell, the opening position is selected from $1/6$ to $5/6$, each at a $1/6$ interval, and the opening sizes are 15, 30, 45, and 60 mm, respectively. A total of 20 models were established. According to the finite element analysis method described in Section 4.1, the characteristic defect of the first-order mode is introduced into the nonlinear buckling analysis in this

section as the initial geometric defect of the conical shell. The geometric defect factor is 10~60% of the shell thickness, and 20% of the shell thickness is selected in this paper. The analysis results are shown in Table 5. At 1/6 and 5/6, the opening with a diameter of 60 mm exceeds the conical shell, so this situation does not participate in the data analysis and discussion. ρ is the ratio of the aperture d_0 to the diameter of the cone where the hole center is located. The critical buckling loads of four apertures at different opening positions. The critical buckling load curves of the four apertures at different opening positions are shown in Figure 12.

Table 5. The critical buckling load of a conical shell with an opening under different opening positions.

Open Position	Model	d_0 (mm)	ρ	P_{cr} (MPa)
1/6	1	15	0.177	2.232
	2	30	0.354	2.178
	3	45	0.531	2.153
	4	60	0.708	-
2/6	5	15	0.160	2.274
	6	30	0.320	2.256
	7	45	0.481	2.206
	8	60	0.641	2.144
3/6	9	15	0.147	2.354
	10	30	0.294	2.292
	11	45	0.441	2.2564
	12	60	0.588	2.130
4/6	13	15	0.135	2.246
	14	30	0.270	2.225
	15	45	0.405	2.201
	16	60	0.540	2.127
5/6	17	15	0.125	2.209
	18	30	0.250	2.194
	19	45	0.375	2.116
	20	60	0.500	-

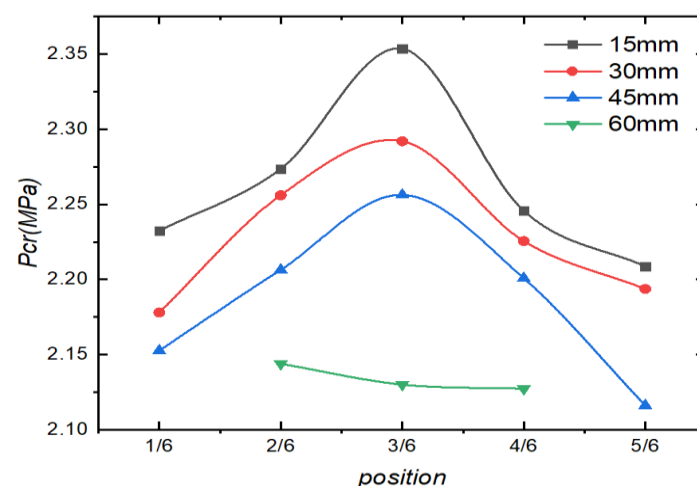


Figure 12. Opening position-critical buckling load curve.

Figure 12 shows that when the opening position is the same, the bearing capacity of the conical shell decreases with the increase in the opening diameter. When the opening rate is less than 0.540, the closer the opening position is to the middle, the greater the critical buckling load is, and the load is the largest when the opening is in the middle position.

When the opening ratio reaches 0.540, the opening position has little effect on the bearing capacity of a conical shell.

Taking the aperture of 30 mm as an example, the following is a set of buckling mode diagrams of reinforced conical shells with openings at positions 1/6, 2/6, 3/6, 4/6, and 5/6, respectively, when the aperture is 30 mm. As shown in Figure 13.

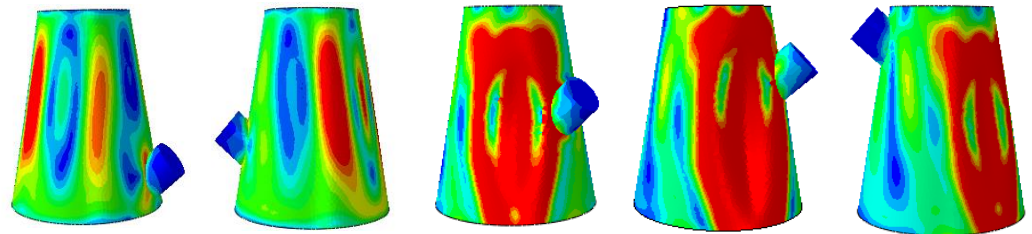


Figure 13. Nonlinear buckling mode of position-critical buckling load.

From Figure 13, it can be seen that the larger stress areas of the five modes are distributed in a block shape. When the opening positions are 3/6 or 4/6, the collapse area mainly surrounds the area near the reinforced enclosure wall. When the opening positions are 1/6, 2/6, and 5/6, the collapse area is all near the opposite side of the reinforced enclosure wall. The position of the opening has a certain impact on the buckling mechanical characteristics of the conical shell strengthened by the opening.

4.3. The Effect of Inclination Angle on Critical Buckling Load under Different Apertures

This section mainly discusses the effect of the inclination angle and opening size on the stability of a conical shell. The opening position is set at 1/2 of the generatrix of the conical shell, the inclination angle of the reinforced wall is selected in the range from 0 to 50°, with an interval of 5°, and the opening sizes are 15, 30, 45, and 60 mm, respectively. A total of 44 models are established to discuss the effect of the inclination angle of the wall and the opening size on the critical load of the conical shell. The analysis results are shown in Table 6. The curves of the critical buckling load values of the four apertures at different wall inclination angles are shown in Figure 14.

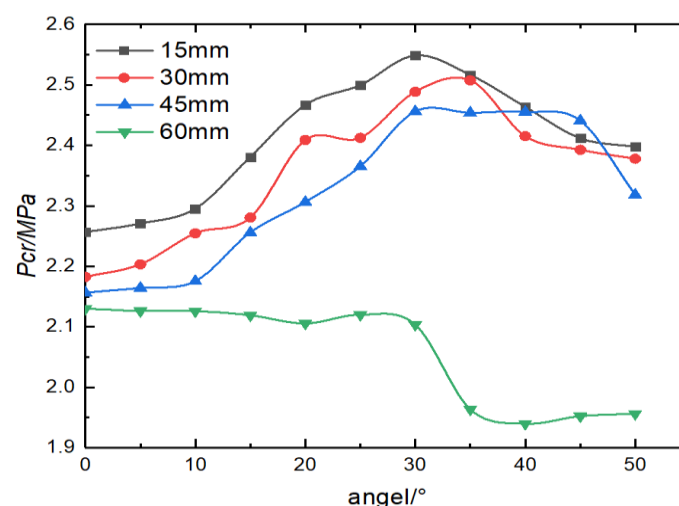


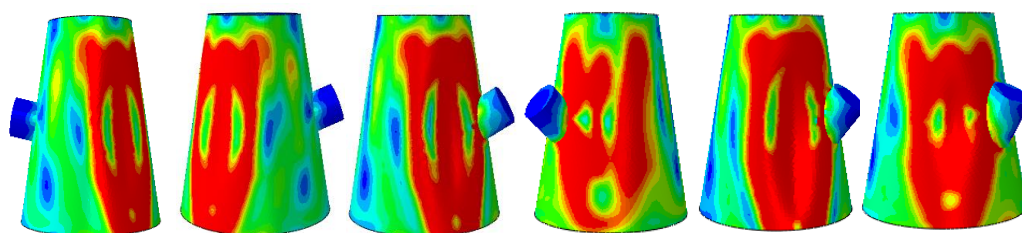
Figure 14. Wall inclination angle-critical buckling load curve.

Table 6. Critical loads of conical shells with an opening at different inclination angles and opening sizes.

α (°)	Model	d_0 (mm)	ρ	P_{cr} (MPa)	α (°)	Model	d_0 (mm)	ρ	P_{cr} (MPa)
0	1	15	0.147	2.257	30	25	15	0.147	2.548
	2	30	0.294	2.182		26	30	0.294	2.488
	3	45	0.441	2.156		27	45	0.441	2.456
	4	60	0.588	2.130		28	60	0.588	2.103
5	5	15	0.147	2.271	35	29	15	0.147	2.516
	6	30	0.294	2.203		30	30	0.294	2.508
	7	45	0.441	2.164		31	45	0.441	2.454
	8	60	0.588	2.126		32	60	0.588	1.964
10	9	15	0.147	2.295	40	33	15	0.147	2.464
	10	30	0.294	2.255		34	30	0.294	2.415
	11	45	0.441	2.175		35	45	0.441	2.455
	12	60	0.588	2.126		36	60	0.588	1.940
15	13	15	0.147	2.381	45	37	15	0.147	2.412
	14	30	0.294	2.281		38	30	0.294	2.393
	15	45	0.441	2.256		39	45	0.441	2.441
	16	60	0.588	2.119		40	60	0.588	1.952
20	17	15	0.147	2.467	50	41	15	0.147	2.397
	18	30	0.294	2.409		42	30	0.294	2.378
	19	45	0.441	2.306		43	45	0.441	2.318
	20	60	0.588	2.105		44	60	0.588	1.956
25	21	15	0.147	2.499					
	22	30	0.294	2.412					
	23	45	0.441	2.365					
	24	60	0.588	2.120					

As can be seen from Table 5 and Figure 14, when the inclined angle of the wall is invariant, the critical load of the conical shell decreases with the increase in the opening diameter. When the opening ratio is less than 0.441, the load of the conical shell increases with the increase in the inclination angle of the wall. When the inclination angle increases to about 30°, the load reaches its maximum value, then gradually decreases and stops at about 45°. However, when the opening ratio reaches 0.588, the critical buckling load of the conical shell reaches its maximum when the inclination angle of the wall is 0°, then it basically shows a straight line, decreases linearly at about 30°, and then tends to be gentle. This finding indicates that small openings, such as some installation equipment or pipelines, can be selected when the wall inclination angle is about 30°. This is basically consistent with the influence of the inclination angle of the wall on the ultimate load of the pipeline in Reference [20]. When opening large holes such as manholes or observation windows, it is more inclined to open vertically.

Taking the aperture of 30 mm as an example, the following is a set of buckling mode diagrams of reinforced conical shells with holes around the angle of the reinforced wall. They are 0°, 10°, 20°, 30°, 40°, and 50° from left to right, as shown in the following Figure 15.

**Figure 15.** Nonlinear buckling mode of angle-critical buckling load.

From Figure 15, it can be seen that the larger stress areas of the six modes are all distributed in a sheet-like manner. When the inclination angle of the reinforcement wall with holes is between 0° and 10° , the collapse area mainly surrounds the sheet-like area opposite the reinforcement wall. When the inclination angle of the reinforcement wall with holes is 20° , 30° , 40° , or 50° , the collapse area mainly surrounds the sheet-like area opposite the reinforcement wall, indicating that as the inclination angle of the wall increases, the stress around the wall is also more pronounced.

5. Conclusions

In this paper, the effects of opening parameters and reinforcing wall parameters on the bearing capacity of a conical shell are studied. The numerical results and the test results of the actual model are compared. The conclusions are as follows:

(1) The difference between the numerical results and the experimental results of 10 conical shells with an opening is within 17.8%. Based on the real geometry, average thickness, and material properties, the nonlinear critical load of the conical shell with an opening can be obtained. The final failure mode obtained by the numerical analysis is consistent with the collapse mode obtained by the hydraulic test of the actual model. The collapsed position of the hydraulic test is the opposite of the opening reinforcement position, indicating the effectiveness of the wall reinforcement on the bearing capacity of the conical shell.

(2) With the increase in opening diameter, the bearing capacity of conical shells shows a decreasing trend. When the opening reinforcement wall is perpendicular to the generatrix of the conical shell and the opening ratio is less than 0.540, the critical buckling load is maximum when the opening is in the middle position. When the opening ratio reaches 0.540, the opening position has little effect on the bearing capacity of a conical shell.

(3) When the opening ratio is less than 0.441, the inclination angle of the wall is about 30° , and the critical buckling load reaches its maximum. Therefore, when some small openings are needed, such as for installation equipment or pipelines, an inclination angle of the wall of around 30° can be selected. When the opening rate reaches 0.588, it shows that the critical buckling load of the conical shell with an opening reaches its maximum when the inclination angle of the wall is 0° . Therefore, when large openings such as manholes or observation windows are opened, they are more inclined to open vertically.

Author Contributions: Conceptualization, methodology and funding acquisition, Y.Z.; Software, validation, formal analysis, writing—original draft preparation, writing—review and editing, L.Y.; Investigation and resources, H.P.; Visualization and project administration, T.S.; Supervision and project administration, J.Z. All authors have read and agreed to the published version of the manuscript.

Funding: This work was supported by the National Natural Science Foundation of China [grant numbers: 52271277], the Natural Science Foundation of Jiangsu Province [grant no. BK20211343], and the State Key Laboratory of Ocean Engineering at Shanghai Jiao Tong University [grant no. GKZD010081].

Informed Consent Statement: Informed consent was obtained from all subjects involved in the study.

Data Availability Statement: In this section, please provide details regarding where data supporting reported results can be found, including links to publicly archived datasets analyzed or generated during the study.

Conflicts of Interest: The authors declare no conflict of interest.

References

1. Shan, L.; Weibo, W. Research status and prospect of pressure hull structure of submersible. *Ship Sci. Technol.* **2019**, *41*, 7–16.
2. Shiping, S.; Jiantang, H.; Weihong, Z. Optimization of opening shape of revolution shell based on hyperelliptic equation and sequential response surface method. *Acta Aeronaut. Sin.* **2015**, *36*, 3595–3607.
3. Teng, J.G.; Zhao, Y.; Lam, L. Techniques for buckling experiments on steel silo transition junction. *Thin Walled Struct.* **2015**, *39*, 685–707. [[CrossRef](#)]

4. Ross, C.T.F.; Little, A.P.F.; Adeniyi, K.A. Plastic buckling of ring-stiffened conical shells under external hydrostatic pressure. *Ocean Eng.* **2005**, *32*, 21–36. [[CrossRef](#)]
5. Wintersetter, T.A.; Schmit, H. Stability of circular cylindrical steel shells under combined loading. *Thin Walled Struct.* **2001**, *40*, 893–909. [[CrossRef](#)]
6. Popov, A.A. Parametric resonance in cylindrical shells: A case study in nonlinear vibration of structural shell. *Eng. Struct.* **2003**, *25*, 789–799. [[CrossRef](#)]
7. Golzan, B.S.; Showkati, H. Buckling of thin-walled conical shells under uniform external pressure. *Thin Walled Struct.* **2008**, *46*, 516–529. [[CrossRef](#)]
8. Cho, S.-R.; Muttaqie, T.; Do, Q.T.; Park, S.H.; Kim, S.M.; So, H.Y.; Sohn, J.M. Experimental study on ultimate strength of steel-welded ring-stiffened conical shell under external hydrostatic pressure. *Mar. Struct.* **2019**, *67*, 102634. [[CrossRef](#)]
9. Chunfang, W. Analysis of stress characteristics of openings in ring-stiffened conical shells. *Electromech. Inf.* **2011**, *12*, 203–204.
10. Kathiresan, M. Influence of shape, size and location of cutouts on crashworthiness performance of aluminum conical frusta under quasi-static axial compression. *Thin Walled Struct.* **2020**, *154*, 106793. [[CrossRef](#)]
11. Debski, H.; Rozylo, P. Experimental study on the effect of eccentric compressive load on the stability and load-carrying capacity of thin-walled composite profiles. *Compos. Part B* **2021**, *226*, 109346. [[CrossRef](#)]
12. Rozylo, P.; Wyszmulski, P. Failure analysis of thin-walled composite profiles subjected to axial compression using progressive failure analysis (PFA) and cohesive zone model (CZM). *Compos. Struct.* **2021**, *262*, 113597. [[CrossRef](#)]
13. Ma, Q. *Opening Reinforcement Design and Experimental Investigation of Spherical Shell for Deep-Sea Submersible*; Jiangsu University of Science and Technology: Zhenjiang, China, 2018.
14. Zhu, Y.; Chen, B.; Zhao, B.; Zhao, X.; Tang, W.; Wang, X. Buckling characteristics of externally pressurised toroidal shell. *Ships Offshore Struct.* **2020**, *15*, 804–814. [[CrossRef](#)]
15. Zhu, Y.M.; Zhang, Y.W.; Zhao, X.L.; Zhang, J.; Xu, X. Elastic-plastic buckling of externally pressurized hemispherical heads. *Ships Offshore Struct.* **2019**, *14*, 829–838. [[CrossRef](#)]
16. Jasion, P.; Magnucki, K. Elastic buckling of clothoidal-spherical shells under external pressure—Theoretical study. *Thin Walled Struct.* **2015**, *86*, 18–23. [[CrossRef](#)]
17. Zhang, J.; Wang, M.L.; Wang, W.B.; Tang, W.; Zhu, Y. Investigation on egg-shaped pressure shells. *Mar. Struct.* **2017**, *52*, 50–66. [[CrossRef](#)]
18. Ifayefunmi, O.; Blachut, J. The effect of shape, boundary and thickness imperfections on plastic buckling of cones. In Proceedings of the International Conference on Ocean, Offshore and Arctic Engineering, Rotterdam, the Netherlands, 19–24 June 2011; Volume 2, pp. 23–33.
19. Zhu, Y.; Yu, J. Effects of the geometrical shapes on buckling of conical shells under external pressure. *Int. J. Press. Vessel. Pip.* **2022**, *196*, 104624. [[CrossRef](#)]
20. Li, N. Study on plastic limit load of internal pressure inclined nozzle structure. *Mech. Strength* **2007**, *29*, 970–974.

Disclaimer/Publisher’s Note: The statements, opinions and data contained in all publications are solely those of the individual author(s) and contributor(s) and not of MDPI and/or the editor(s). MDPI and/or the editor(s) disclaim responsibility for any injury to people or property resulting from any ideas, methods, instructions or products referred to in the content.